Understanding the Dependence of Satellite Rainfall Uncertainty on Topography and Climate for Hydrologic Model Simulation

Abebe S. Gebregiorgis and Faisal Hossain

***Abstract*—A quantitative and physical understanding of satellite rainfall uncertainties provides meaningful guidance on improving algorithms to advance hydrologic prediction. The aim of this study is to characterize satellite rainfall errors and their impact on hydrologic fluxes based on fundamental governing factors that dictate the accuracy of passive remote sensing of precipitation. These governing factors are land features—comprising topography (elevation)—and climate type, representing the average ambient atmospheric conditions. First, the study examines satellite rainfall errors of three major products, 3B42RT, Climate prediction center MORHing technique (CMORPH), and Precipitation Estimation from Remotely Sensed Information using Artificial Neural Networks (PERSIANN), by breaking the errors down into independent components (hit, miss-rain, and false-rain biases) and investigating their contribution to runoff and soil moisture errors. The uncertainties of three satellite rainfall products are explored for five regions of the Mississippi River basin that are categorized grid cell by grid cell (at the native spatial resolution of satellite products) based on topography and climate. It is found that total and hit biases dictate the temporal trend of soil moisture and runoff errors, respectively. Miss-rain and hit biases are the leading errors in the 3B42RT and CMORPH products, respectively, whereas false-rain bias is a pervasive problem of the PERSIANN product. For 3B42RT and CMORPH, about 50%–60% of grid cells are influenced by the total bias during winter and 60%–70% of grid cells during summer. For PERSIANN, about 70%–80% of the grid cells are marked by total bias during the summer and winter seasons. False-rain bias gradually increases from lowland to highland regions universally for all three satellite rainfall products. Overall, the study reveals that satellite rainfall uncertainty is dependent more on topography than the climate of the region. This study's results indicate that it is now worthwhile to assimilate the static knowledge of topography in the satellite estimation of precipitation to minimize the uncertainty in anticipation of the Global Precipitation Measurement mission.**

***Index Terms*—Climate, precipitation, remote sensing, satellite, topography, uncertainty.**

Manuscript received November 5, 2011; revised February 14, 2012 and March 30, 2012; accepted April 15, 2012. This work was supported by the NASA New Investigator Program (NIP) Grant NNX08AR32G of Faisal Hossain. The work of A. S. Gebregiorgis was supported in part by the National Aeronautics and Space Administration (NASA) NIP Grant NNX08AR32G of Faisal Hossain and in part by the Center for the Management, Utilization and Protection of Water Resources at Tennessee Technological University.

The authors are with Tennessee Technological University, Cookeville, TN 38505 USA (e-mail: abesine2002@yahoo.com; fhossain@tntech.edu).

Color versions of one or more of the figures in this paper are available online at http://ieeexplore.ieee.org.

Digital Object Identifier 10.1109/TGRS.2012.2196282

I. Introduction

As PRECIPITATION (hereafter used synonymously with "rainfall") is the key factor in hydrologic model simulation [1]–[3], determining the uncertainty of satellite precipitation estimation has fundamental importance for many applications. Quantifying and characterizing error in rainfall estimates provide meaningful information in the short- and the long-term monitoring of water-driven processes such as weather forecasting [4]–[7], flood monitoring and control [8], [9], agriculture and drought monitoring [10], [11], climate research and prediction [12], [13], and hydrological and water resource planning [14], [15]. Satellite rainfall uncertainty (hereafter used synonymously with "errors") analysis can range from a simple error source description [16], [17] to complex methods of quantification and propagation in hydrologic models [2], [18]–[21].

Several studies have been conducted on satellite rainfall uncertainty [1], [2], [16], [17], [21]–[27]. For example, Nijssen and Lettenmaier [1] pointed out that the major sources of uncertainty in satellite rainfall products arise from sampling, instrumental, and algorithmic errors. In particular, sampling error contributes considerably to satellite rainfall uncertainty and can occur due to the location of satellite orbit, size of swath width, and spatial and temporal mismatch between satellite and reference rainfall fields. In another study, Hossain and Anagnostou [28] developed a satellite rainfall error model to understand the propagation of errors for passive microwave (PMW) and infrared (IR) products by corrupting a more accurate ground rainfall measurement. By considering a realistic IR retrieval scheme and merging it with simulated PMW retrievals, they studied the effect of satellite rainfall uncertainty on hydrologic prediction. The study underscored the need for more frequent sampling and merging of IR and PMW rainfall estimates to reduce the uncertainty in satellite-based flood prediction.

Tian *et al.* [17] developed a scheme to break down the total bias of satellite rainfall precipitation into hit bias, miss-rain bias (missed precipitation), and false-rain bias (false precipitation) for the contiguous United States. A hit (H) is defined as a record of rainfall (greater than a threshold value, usually 1 mm/day according to Tian *et al.* [17]) reported by both satellite and validation (ground) data. The difference between these records (satellite minus ground observations) is a hit bias. A miss (M) occurs when the satellite product documents no rain during actual rain condition, whereas if the satellite data report rain but it is not verified by the ground data, then it is called a

false precipitation (F). These error components are mutually independent and closely related to satellite retrieval stages: signal detection (screening) and rain rate estimation. Missed and false precipitations are the possible error components that can occur during the screening stage (identifying rain/no-rain areas), and hit bias can occur due to weak signal, such as cloud-top temperature which has a weak physical link to rainfall processes and cloud optical properties. The study [17] advocated that error decomposition can distinguish the source of bias and identify the sources of error components that contribute to the total bias. These error components can sometimes cancel each other due to opposite signs to yield smaller total bias and sometimes add up together to increase larger total bias [17]. Thus, such breaking down of error helps to gain an in-depth understanding of error sources tied to the retrieval process, which eventually guides data producers and algorithm developers toward appropriate adjustment and correction.

Gebregiorgis *et al.* [21] addressed the effect of three error components (hit, miss-rain, and false-rain biases) of satellite rainfall products on hydrologic simulation based on land use and land cover (LULC) condition. This breaking down of satellite rainfall error allowed the tracing back of simulated hydrological fluxes and states to the source of error components. Using the entire Mississippi River basin (MRB) as the study region and the variable infiltration capacity (VIC)-3L as the distributed hydrologic model [39], the study of the satellite products (CMORPH [44], 3B42RT [42], and PERSIANN [45]) yielded two key findings. First, during the winter season, more than 50% of the rainfall total bias was found to be dominated by missed precipitation in forest and woodland regions (southeast of Mississippi). During the rainy season, 45% of the total bias was governed by the hit bias, and about 28% was governed by the false precipitation in grassland–savanna region (west part of the Mississippi basin). Second, a strong dependence was observed between hit bias and runoff error and missed precipitation and soil moisture.

Herein, it is important to highlight the physical insight that the study of LULC provides. First, LULC has an impact on satellite rainfall retrieval algorithm because of the surface emissivity variation for different land cover systems. Hewison [29] operated low-level aircraft that carried a PMW radiometer over an area characterized by different vegetation covers. His study revealed a strong correlation between background surface emissivity and vegetation cover. Based on this study, bare soil displayed high emissivity with very little polarization contrast, close conifer forest showed very high emissivity at all frequencies with no polarization difference, and the remaining forest group exhibited low emissivity at lower frequencies. Such emissivity variation due to LULC diversity can be sufficiently large to affect the retrieval process during satellite rainfall estimation process. In satellite-based rainfall estimation, it is well known that different products use information from IR and PMW spectral bands in their retrieval algorithms. However, surface emissivity specifically affects the PMW retrievals, and that in turn affects the algorithms' performance only to the degree to which the PMW retrievals contribute in each case. Therefore, CMORPH (which uses purely PMW), 3B42RT (which uses mainly PMW), and PERSIANN (which uses only IR calibrated against PMW) should be affected to various degrees by the surface emissivity variations. In principle, even though the calibrated IR should reflect the average behavior of PMW, differing levels of sensitivity to surface emissivity in retrieval techniques are unavoidable. In addition, *to what extent does surface emissivity affect the retrieval process of the three products* is also an interesting science question but is not the focus of this study.

Second, LULC has a significant impact on the transformation of incoming rainfall into direct runoff, percolation, and infiltration. For instance, forest and woodland systems facilitate more percolation and infiltration processes than runoff generation at the beginning of a storm, whereas human land use (crop land system) facilitates the formation of runoff rather than the infiltration process [21]. Thus, it is not surprising that LULC-based studies of uncertainty reveal clear patterns (such as [21]) that should to be acknowledged if the estimation and application of satellite rainfall products are to be advanced.

In addition to LULC, land features, such as topography, can play a profound role on the formation and type of precipitation at global, regional, and local scales [30]. For instance, the literature indicates that satellite rainfall estimation over mountainous regions or complex terrains remains a challenge [31]–[35]. In the case of the IR spectral range, clouds are opaque, and precipitation is estimated from cloud-top temperature that is related to cloud height. Such a retrieval heuristic can often miss warm and orographic rainfall in mountainous regions [36]. Moreover, this IR heuristic based on cloud-top temperature undermines stratiform clouds that can be warm but rain bearing and overvalues cirrus clouds that are not as rain bearing. Similarly, the PMW retrieval algorithm comes from two signal detection methods: ice scattering and emissivity. In the case of ice scattering, the rainfall rate is associated with the amount of ice in clouds, but warm orographic clouds in tropics can produce substantial rainfall with little or no ice, which could lead to missed precipitation by PMW sensors. On the other hand, as surface emissivity is sensitive to land cover, as discussed earlier, the background emissivity signal that comes from cold surfaces and ice cover over mountainous regions may sometimes be identified as rain, which could lead to false precipitation (i.e., false-rain bias).

It is apparent from the aforementioned review that satellite rainfall uncertainty studies have so far explored issues such as sampling [1], retrieval [28], and, more recently, geophysical features such as LULC [21]. However, other accompanying geophysical features such as topography and climate, which can collectively control surface emissivity (e.g., lower surface temperature at higher altitudes or sparse vegetation at semi-arid climates), have not been investigated in detail. Herein, we refer to topography as "elevation" or "altitude" and climate according to the standard Koppen climate classification [38]. These two features are neither dependent nor mutually exclusive of LULC that has been recently studied [21]. In many places, LULC data can be an unreliable feature because of outdated land surveys or recent and rapidly evolving land cover change due to human settlement. However, topography and climate are relatively "stable" as features and therefore deserve an equally detailed investigation if future application of satellite

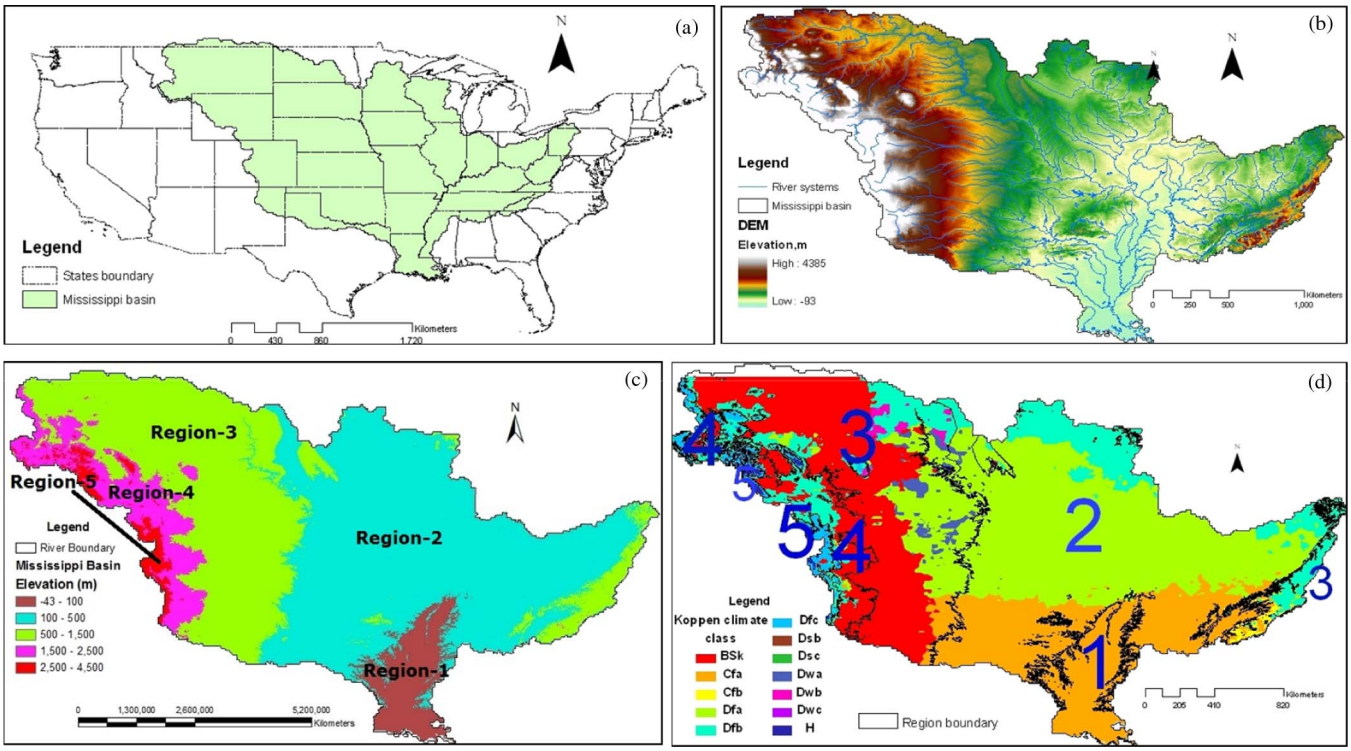

Fig. 1. (a) Geographic location, (b) digital elevation model of the study basin, (c) elevation-based categorized regions, and (d) overlay of region boundary [the numbers indicate the corresponding regions shown in (c)] and Koppen climate classes (http://koeppen-geiger.vu-wien.ac.at) of the Mississippi basin (Table I—detail description of Koppen climate classes).

precipitation data is to be improved on the basis of optimal merging according to the *a priori* hydrologic predictability of the data product. The study of Gebregiorgis and Hossain [37] on the optimal merging of various satellite rainfall data sets revealed that a detailed understanding of the range of geophysical controls of satellite rainfall uncertainty for each grid box is necessary to improve application over ungauged regions where *in situ* data are nonexistent.

Given that there has historically been no study of the dependence of topography and climate on satellite rainfall uncertainty, this paper is intended to address the following two key questions.

1) *How do rainfall total bias and error components of satellite products vary with different topography and climate features?*
2) *How does the topography or climate-dependent uncertainty of satellite rainfall products affect the simulation of hydrological fluxes and states?*

As a broader impact, answers to the aforementioned question are directly relevant to improving satellite rainfall estimation. By leveraging the *a priori* uncertainty of three different near-real-time satellite rainfall products (3B42RT, CMORPH, and PERSIANN), Gebregiorgis and Hossain [37] have devised a merging method to produce a more accurate and superiorly merged product. To implement such a multiproduct merging approach in regions where observation data are often nonexistent or sparse, derivation of these *a priori* estimates of uncertainty from commonly available information is required. Thus, the understanding of uncertainties based on climate and topographic features stands to afford the transfer of error information to an ungauged basin where ground-truth data are unavailable [27]. This paper is organized as follows. The study area, data, and methodology are presented in Section II. Major findings and analysis of results are introduced in section III. Finally, in Section IV, the conclusion and possible recommendations are described.

TABLE I
KÖPPEN CLIMATE CLASSES FOR MRB [38]

Group	Types	Köppen climate features
B	BSk	Arid-steppe (cold)
C	Cfa	Temperate-without dry season (hot summer)
D	Dfa	Cold-without dry season (Hot summer)
	Dfb	Cold-without dry season (warm summer)
	Dfc	Cold-without dry season (cold summer)

II. STUDY AREA, DATA, MODEL, AND METHOD

A. Study Area

The study was conducted in the MRB which is the largest basin in North America and the third largest drainage basin in the world next to the Amazon and Congo Rivers [see Fig. 1(a)]. MRB encompasses more than 40% of the U.S. land area, extending from the Allegheny Mountains in the east to the Rocky Mountains in the west. Due to its diverse physiographic conditions ranging from lowland and flat floodplains to high mountains [see Fig. 1(b) and (c)] and different climate features [see Fig. 1(d)], MRB has been selected as a test bed for this particular study.

TABLE II
SUMMARY OF SATELLITE AND GAUGED RAINFALL DATA SETS FOR THE STUDY

Dataset	Description	Sensors product	Native spatial resolution	Native temporal resolution	References
3B42RT	TRMM Multisatellite Precipitation Analysis Real-time experimental product	Merged product of calibrated-IR and MW	0.25°	3 hrs	[42], [43]
CMORPH	NOAA Climate Prediction Center (CPC) MORPHing technique	MW product but IR used to derive cloud motion field	0.25°	3 hrs	[44]
PERSIANN	Precipitation Estimation from Remotely Sensed Information using Artificial Neural Networks - Cloud Classification System	MW calibrated IR product	0.04	1 hr	[45] - [48]
GGRD	University of Washington - gridded ground rainfall data	Gridded from gauge observation	0.125	1 day	[40]

For this study, the MRB was classified into different regions based on topography and climate conditions. According to topography of the area (i.e., elevation), it was grouped into five different regions as follows: lowland/region 1 [elevation ranging from 0 to 100 m above sea level (a.s.l)], region 2 (elevation ranging from 100 to 500 m), region 3 (elevation ranging from 500 to 1500 m), region 4 (elevation ranging from 1500 to 2500 m), and highland/region 5 (elevation ranging from 2500 to 4500 m) [see Fig. 1(c)]. Although 12 different Koppen climate classes are present in the MRB [38], only the five most dominant classes that cover most of the basin area were considered [see Fig. 1(d) and Table I].

B. Study Data and Hydrologic Model

Three near-real-time satellite rainfall products (3B42RT, CMORPH, and PERSIANN) were used to simulate runoff and soil moisture over the Mississippi basin. The VIC-3L macroscale hydrologic model [39] was implemented at a 0.125° spatial resolution and daily temporal scale during the three-year study period (2003–2005). The start of the study period (2003) was selected because this period was the first operational year for the three products. On the other hand, the end period of the study was considered to be 2005 due to the fact that VIC input gridded meteorological driving data sets were available only for the period spanning from 1915 to 2005 at the time of writing and revising this manuscript (early 2011). Given that the study period 2003–2005 is closer to the start of all three satellite algorithms than to their present forms, the impact of the study may be limited on the extent of the existing algorithm improvements which must be highlighted as the limitation of this study. The gridded ground observation data sets obtained from the University of Washington [40] were used for model calibration and validation and as reference data set for error computation. Using these reference data sets and calibrated model, the runoff and soil moisture were simulated and considered as synthetic truth data to evaluate the runoff and soil moisture errors of satellite rainfall products by taking hydrological model errors into account. Detailed descriptions of the data sets were summarized in Table II. The reader is also referred to [37] and [21] for further details on the VIC-3L model setup over MRB.

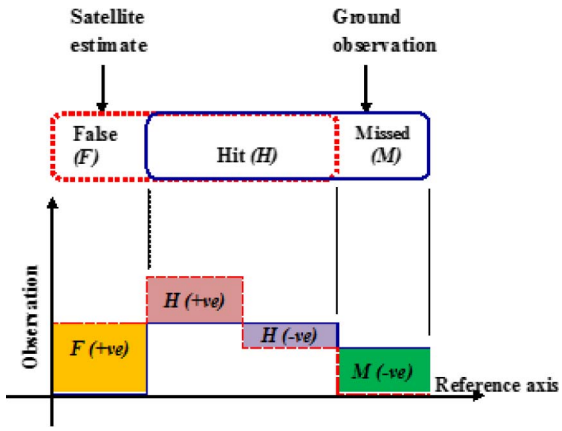

Fig. 2. Schematic representation of satellite rainfall error components, hit bias (H), missed precipitation (M), and false precipitation (F), relative to ground-truth observation.

C. Method

Tian *et al.* [17] and Habib *et al.* [41] have demonstrated a method of breaking down the total rainfall bias into three independent components consisting of the bias associated with successful detection (hit), bias due to missed precipitation, and bias due to false detections. Fig. 2 illustrates the schematic representation of the error decomposition concept for satellite rainfall observation relative to ground validation data. The left region on Fig. 2 shows the outcomes of false alarm. In this case, the satellite detects a rainfall event actually where there is no rain on the ground. Hit occurs when both satellite and reference data report rainfall coincidently. If the rainfall estimates in both cases are the same, then it is a successful detection; otherwise, it is a hit bias. On Fig. 2, the middle region represents the occurrence of hit outcomes in which the bias could be negative, positive, or zero. The occurrence of such error is realistic during

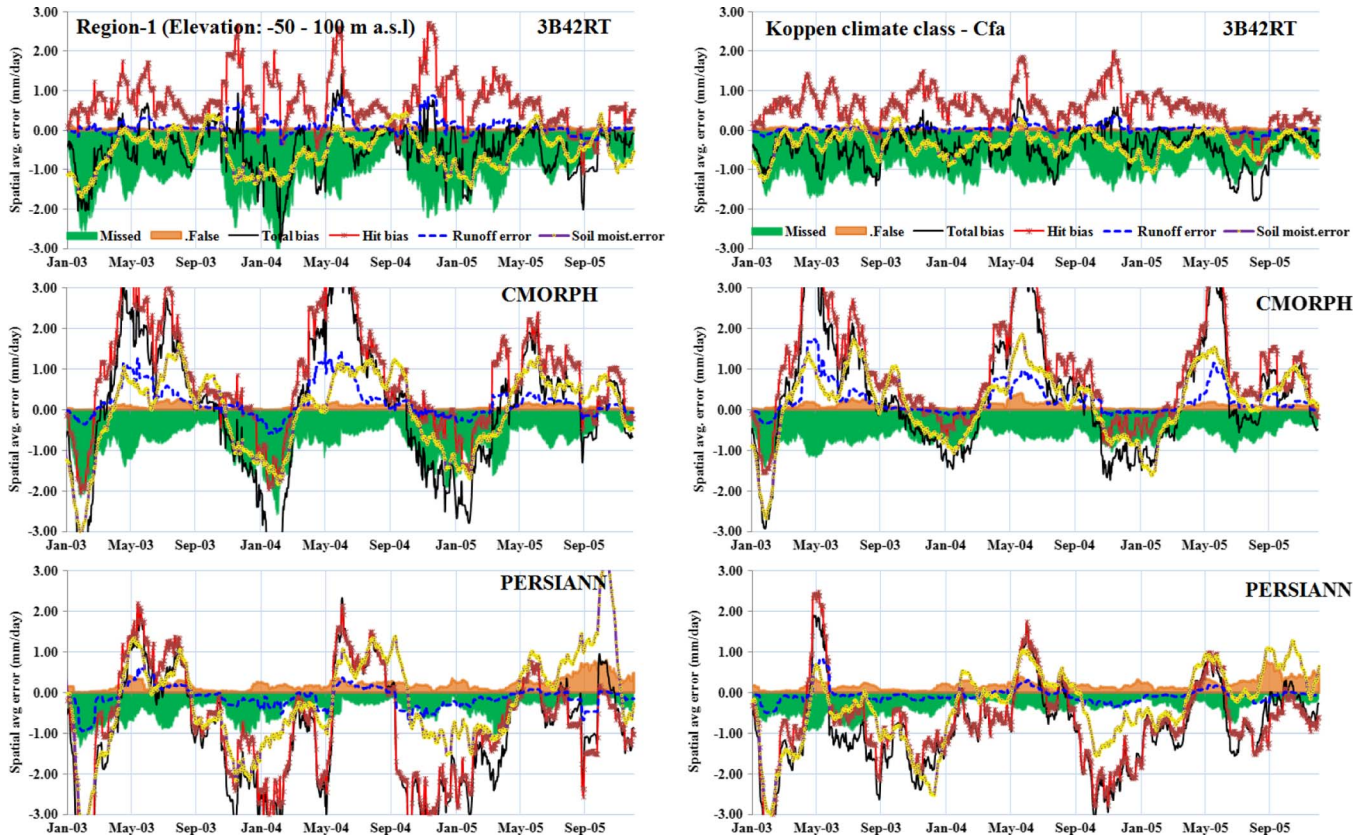

Fig. 3. Time series of error components of three satellite rainfall products and simulated soil moisture and runoff errors for (left panels) lowland region and (right panels) Cfa Koppen climate class. In this case, the lowland region is characterized as elevation below 100 m a.s.l. Cfa class is distinguished as humid subtropical region (see Fig. 1 for detail description). Line/area color description: Dark line—total bias; red line—hit bias; blue line—runoff error; green line—soil moisture error; orange shade—false precipitation; turquoise shade—missed precipitation.

the second stage of retrieval process (rain estimation). On the other hand, the satellite could fail to detect the rain event that is actually happening on the ground and such outcome is called missed rainfall (Fig. 2, right region). Both outcomes (missed and false precipitations) occur during the first stage of retrieval process (screening) and always contribute a positive and a negative bias, respectively.

The total bias can be expressed as a sum of three independent bias components. Such decomposition helps to distinguish the contribution of each error component for the formation of the total bias. The error components can sometimes be canceling each other to give the small value of the total bias and, at other times, can add up to build up the total bias [17]. Thus, to get more insight of the error source during satellite retrieval process, such an approach has remarkable contribution toward improving the estimation procedure and understanding the error source. For the reader, a general description of the error decomposition scheme with the appropriate mathematical illustration is presented in Appendix.

III. Result Analysis

The result of the study is presented on two key aspects. The first aspect focuses on the temporal error characteristics and variation (rainfall error components, runoff, and soil moisture errors) based on topography (elevation) and climate conditions (see Figs. 3–5). The error components for each product are spatially averaged within the given region on a daily time scale for the entire study period (2003–2005). In general, this section deals with the volume of magnitude of each error component in time. The second aspect discusses the spatial distribution of rainfall error components, runoff, and soil moisture errors. It focuses on the area magnitude (extent of area coverage) of each error component on a seasonal basis.

A. Temporal Nature of Error Characteristics (Volume Magnitude of Errors)

To remove cluttering, a 31-day moving average is applied for the temporal error trend analysis (see Fig. 3). On the graph, the turquoise and orange shades are the missed and the false precipitation, respectively. The black, red, blue, and green lines represent the total bias, hit bias, runoff error, and soil moisture error, respectively. Fig. 3 shows the trends of time series of satellite rainfall error components, simulated runoff, and soil moisture errors for lowland regions (0–100 m a.s.l) (left) and Cfa Koppen climate class (temperate without dry season) (right) for three satellite rainfall products: 3B42RT (top), CMORPH (middle), and PERSIANN (bottom). For all products, both regions have similar error trends. The 3B42RT product displays significant miss-rain bias with high amplitude during the winter season. The miss-rain bias is consistently reduced for the CMORPH and PERSIANN products. On

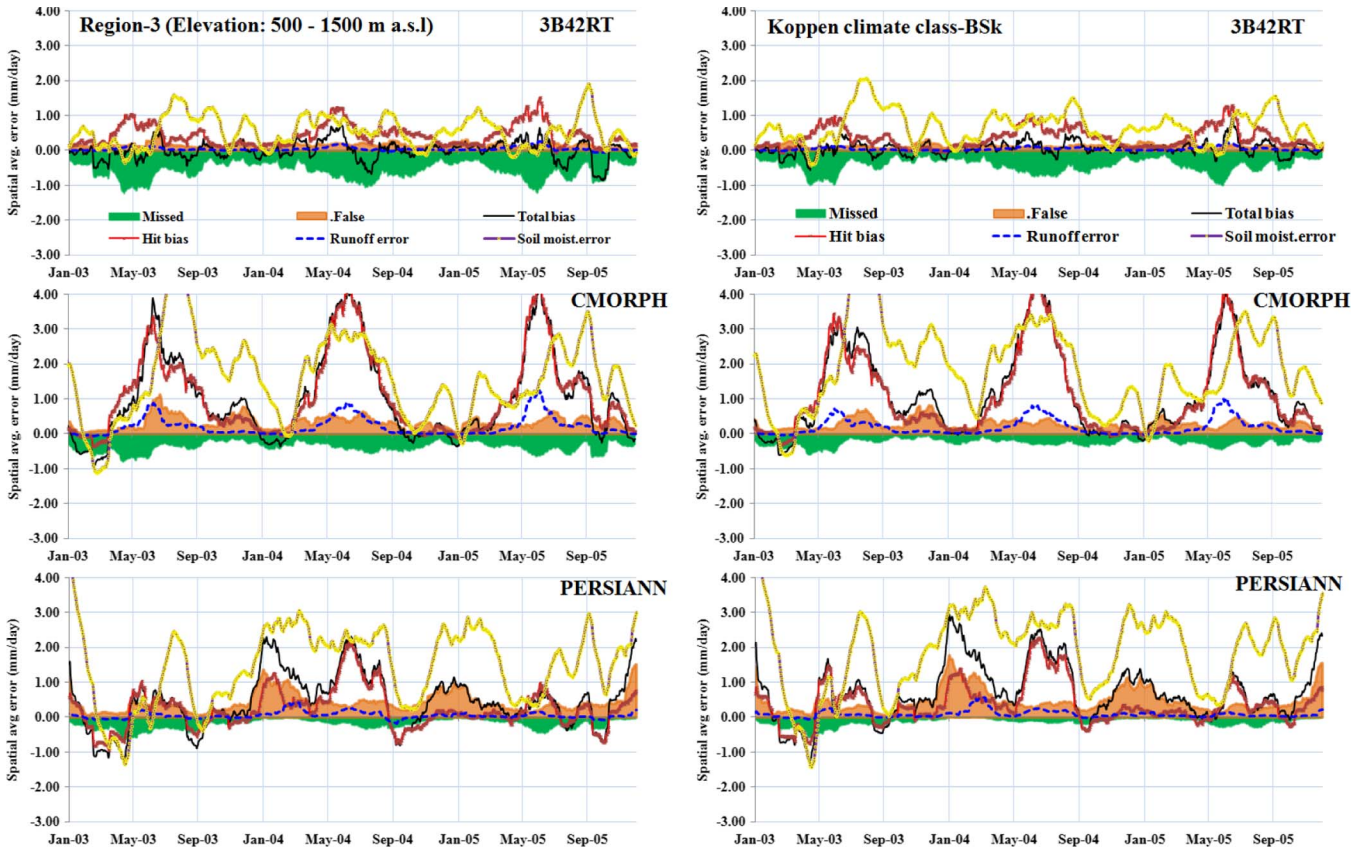

Fig. 4. Same as Fig. 3, except for land feature between (left panels) 500–1500-m altitude and (right panel) midlatitude steppe dry (BSk) climate region.

the other hand, 3B42RT is characterized by positive hit bias throughout the study period but less in magnitude than the missed precipitation. Therefore, for this product, the total bias is totally dominated by miss-rain bias.

For the CMORPH and PERSIANN products, the trends of total and hit biases are similar (wave-shaped trend). Both errors have peak positive during summer and dip negative during winter time. As the magnitudes of miss-rain and false-rain biases are smaller, the total bias is totally dominated by hit bias for both products. False-rain bias is almost negligible in case of 3B42RT and fairly noticeable in the PERSIANN product. In general, false precipitation is not the main challenge for all products in lowland region. From visual observation (on Fig. 3), interestingly, the runoff error follows the trend of hit bias, and soil moisture error maintains the pattern of total bias. The soil moisture error is negative for the 3B42RT product in most cases due to missed precipitation, whereas the runoff error is positive during the same period because of significant amount of hit bias. This proves the strong correlation of runoff with hit bias and soil moisture with miss-rain bias. In case of CMORPH and PERSIANN, similar to the trend of the total bias and hit bias, the soil moisture error has positive error during the summer and drops to negative during the winter season.

Fig. 4 illustrates the temporal trends of rainfall, runoff, and soil moisture error for two regions characterized by an altitude of 500–1500 m a.s.l and BSk climate class (Koppen climate: arid steppe and cold). Even though miss-rain bias is lower in these regions as compared to the lowland areas, there is still significant variation across the three products; miss-rain bias is enhanced in case of 3B42RT and diminished for the PERSIANN product. On the other hand, while significant false-rain bias is observed in the PERSIANN product, 3B42RT reflects the lowest false-rain error.

In all these regions, the total error is largely dominated by hit bias for CMORPH and PERSIANN during the summer season. Therefore, like Fig. 3, the soil moisture error has a similar trend with total bias and hit bias for these two products. Furthermore, in the CMORPH and PERSIANN products, the amplitude of soil moisture error is greater than the magnitude of rainfall error components. We speculate that the reason for high soil moisture error is linked with the occurrence of a considerable amount of false precipitation in these two products, as Gebregiorgis *et al.* [21] have recently reported. False precipitation leads to the overestimation of rainfall that is eventually converted to snow depth at intermediate and high altitude regions by the model, particularly for the winter season. As a result, a large amount of positive error is introduced into simulated soil moisture. In addition, during the summer and early fall months, due to continuous overestimation of rainfall (positive hit bias), the simulated soil moisture remains significantly high.

As seen in Fig. 5, the temporal error trend of highland region (elevation ranging from 2500 to 4000 m a.s.l) and Dfc Koppen climate class (cold without dry season) have many characteristics in common with the previous regions. The drifts of false-rain bias, hit bias, and total bias are some of the

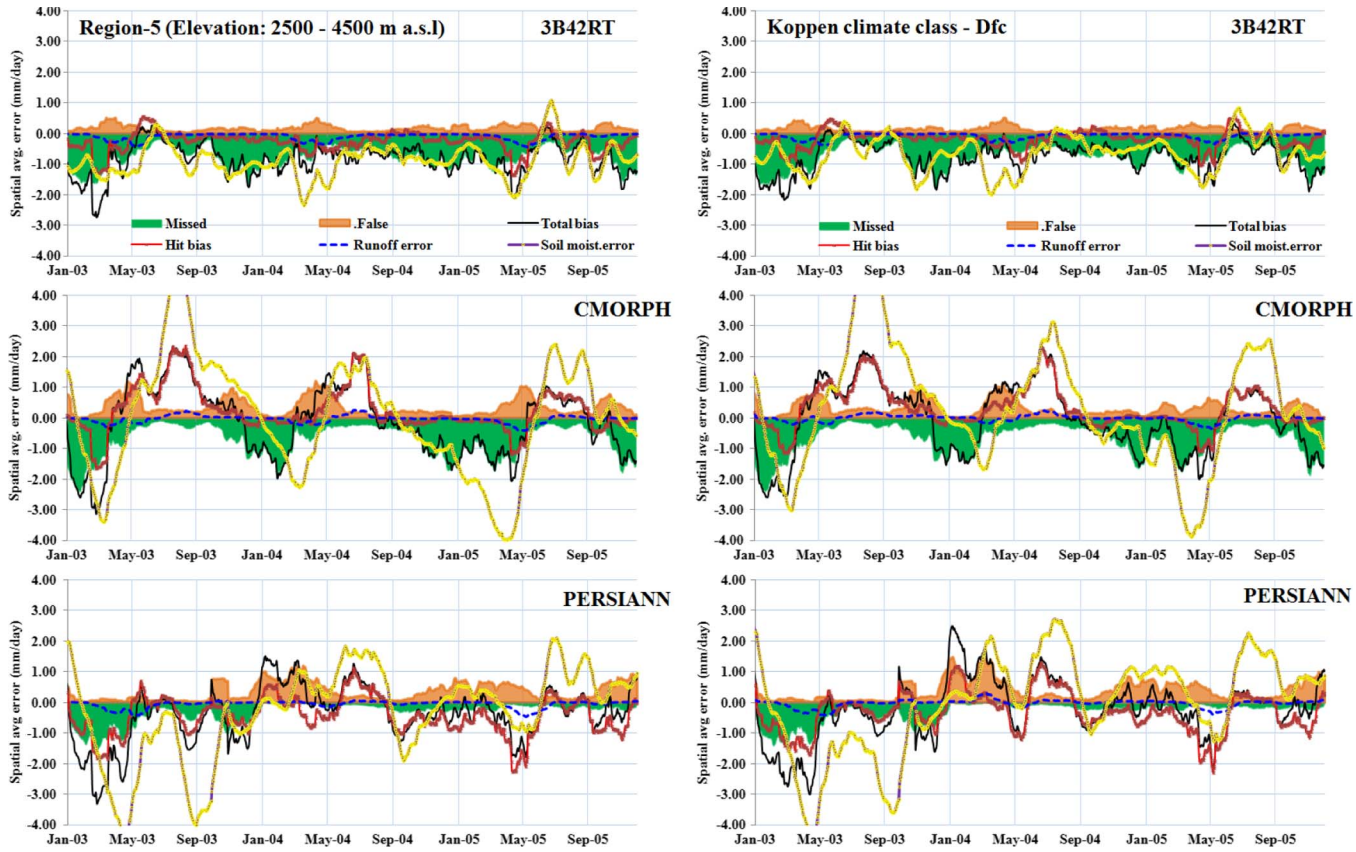

Fig. 5. Same as Fig. 3, except for (left panel) highland regions and (right panel) Dfc Koppen climate class.

common features. For the Dfc Koppen climate class, the missed precipitation of CMORPH has increased for the winter and spring seasons; consequently, it leads the soil moisture error to drop to negative during these seasons.

Overall, the temporal aspect of the study reveals the following key findings. False-rain bias gradually increases from lowland to highland regions consistently for all products, although the sensitivity is less for 3B42RT and much large for the PERSIANN product. This finding leads us to the following rules for improving satellite rainfall estimation. First, false precipitation is the main challenge for all satellite rainfall products in the midaltitude and mountainous (highland) regions and should be minimized if the products are to improve in these regions (see Figs. 4 and 5). We think that the existence of long-lasting orographic clouds over mountain peaks leads to false precipitation. Misdetection of clear and cold surface as precipitating cloud over land and sea surfaces can also result in false-rain bias. Second, the sensor type and technique of retrieval algorithm may play a key role on the magnitude of false precipitation of each product. PERSIANN, which is based on the IR sensor, shows the highest false-rain bias, while 3B42RT, which is merged from IR and PMW, has the least false precipitation. CMORPH (an essentially PMW product) shows some high value of false precipitation during summer season but generally experiences low false precipitation as 3B43RT (see Figs. 4 and 5).

Another aspect of this study is the existence of correlation of rainfall error components with runoff and soil moisture errors. The runoff error is found to be strongly correlated with the hit bias with a correlation coefficient above 0.80 (Fig. 6, left panels). When the hit bias is the dominant error, the runoff error exhibits a strong correlation with the total bias. Correlation coefficients are also found to diminish progressively (even negative with false precipitation in some cases) from lowland to highland region (see Fig. 6). This indicates the changing dependence of errors because of the complex climatic and hydrologic processes over highland regions.

Likewise, the soil moisture error is highly correlated with the total bias (Fig. 6, right panels). From this, we can infer that soil moisture error is affected by all error components. For instance, for PERSIANN, where false precipitation is significant, the soil moisture is equally correlated with false precipitation as it does with the other error components (Fig. 6, right lower panel).

B. Spatial Nature of Error Characteristics (Area Magnitude of Errors)

The spatial coverage and distribution of each error component, including the runoff and soil moisture error, are analyzed as a percentage of the total number of grid cells by counting the pixels for the respective errors. The analysis result includes only lowland (elevation ranging from 0 to 100 m a.s.l) and highland (from 2500 to 4500 m a.s.l) for the winter and summer seasons. Fig. 7 presents the percentage of grid cells dominated by each type of error for lowland region of winter and summer seasons. For the winter season (upper six panels), for 3B42RT and CMORPH, most of the grid cells are controlled by negative total bias due to significant missed precipitation in the region, whereas for the PERSIANN product, the dominance of negative

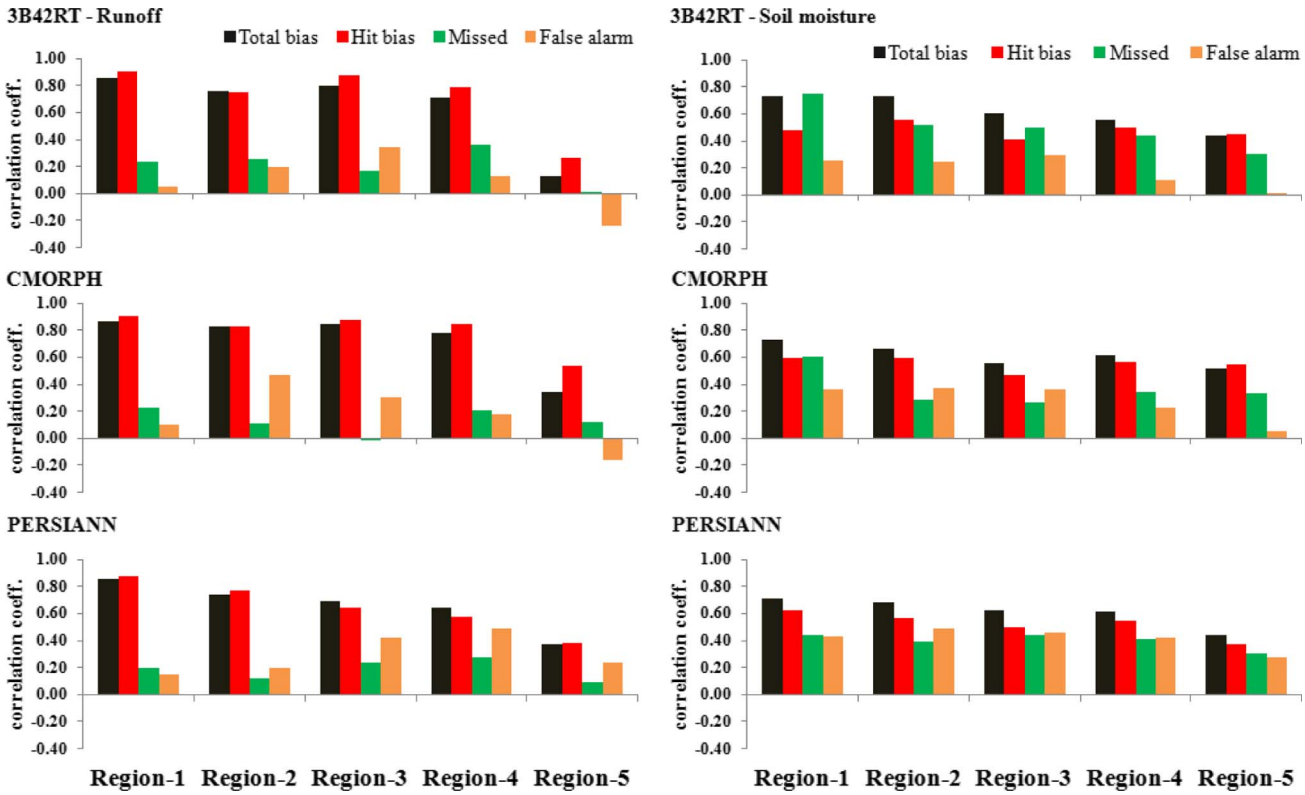

Fig. 6. Correlation coefficient of soil moisture and runoff errors with total bias and rainfall error components for topography-based regions.

total bias reduces due to the large number of false precipitation pixels. The reason for such significant size of missed precipitation in lowland region is attributed to the short-lived storms that are a challenge for PMW sensors due to the infrequent sampling time. As rainfall estimates are derived from PMW for CMORPH and 3B42RT, missed precipitation is expected from these two products. Given the fact that the 3B42RT product uses pure PMW in most grid boxes and IR in others, it should have less missed precipitation than the CMORPH product. However, the higher missed precipitation for the summer season can probably be attributed to the lack of proper IR calibration in 3B42RT. In addition, the percentage of negative hit bias grid cells is found to be larger than that of the positive hit bias grid cells. This shows that PERSIANN underestimates rainfall in large areas even during successful rainfall detection. By large, negative runoff and soil moisture errors dominate the region due to missed precipitation for 3B42RT and CMORPH and due to negative hit bias for PERSIANN. For the summer season, the area coverage of missed precipitation notably reduced for all products.

Fig. 8 illustrates the percentage of areal coverage of errors in highland region (elevation ranging from 2500 to 4500 m a.s.l). About 45% of the region is characterized by miss-rain bias for the 3B42RT and CMORPH products in the highlands during the winter season. Consequently, the negative total bias dominates the region by large. Surprisingly, for these two products, the extent of hit bias is limited to a very small fraction of grid cells. This proves that the major challenge of 3B42RT and CMORPH is missed precipitation in the highland region during the winter season. As pointed out by Tian *et al.* [17], this could be due to the inability of PMW sensors to detect rainfall over snow-covered areas or due to low-level warm rain which may not have a strong signature of ice particles to be detected by the scattering channels. The other possibility is that developers could probably shed light on how the old-version algorithms performed over snowy surfaces for the study period (2003–2005). Unlike the 3B42RT and CMOPRH products, a large percentage of grid cells are dominated by hit bias error for PERSIANN.

The differences in performance among these products lead us to the following conclusions. During the winter (snow) season, for 3B42RT and CMORPH, the problem of missed precipitation is linked to the weakness of screening strategies which fails to discriminate rain from no-rain event. However, the PERSIANN has a weakness during both retrieval stages (screening and estimation). The false precipitation is related to the screening process, and hit bias is linked to the lack of physical correlation between the rain rate and detected signal of cloud-top temperature.

In terms of spatial coverage, on average, 50%–60% and 60%–70% of pixels were influenced by the total bias during winter and summer, respectively, for both 3B42RT and CMORPH. Out of these grid cells, 30%–35% were labeled by miss-rain bias during winter, and 30%–65% were marked by hit bias during summer. For the PERSIANN product, about 70%–80% of the grid cells were marked by total bias during the summer and winter times. For PERSIANN, 45%–50% of the pixels were labeled by hit bias during summer, and 20%–40% were pronounced by false-rain bias during the winter. In general, for the PERSIANN product, hit bias and

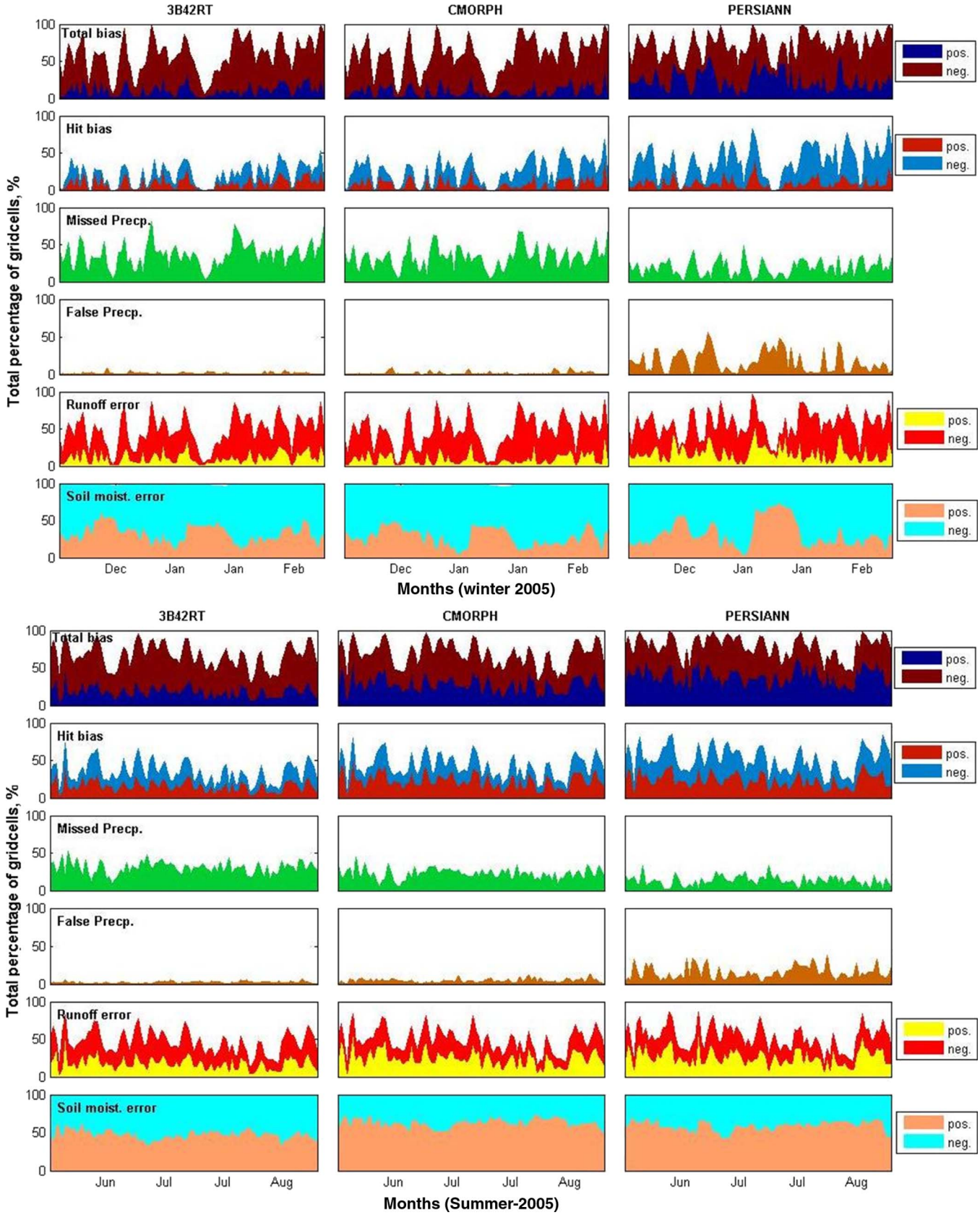

Fig. 7. Percentage of grid cells dominated by various rainfall error components and soil moisture and runoff errors for lowland region for (top six panels) winter and (bottom six panels) summer of 2005.

false-rain bias were the major error contributors for the total bias in terms of the areal coverage during summer and winter seasons, respectively. For 3B42RT and CMORPH, hit bias and miss-rain bias were the dominant error sources for the summer and winter seasons, respectively. The overall percentage of error distribution is presented in Table III.

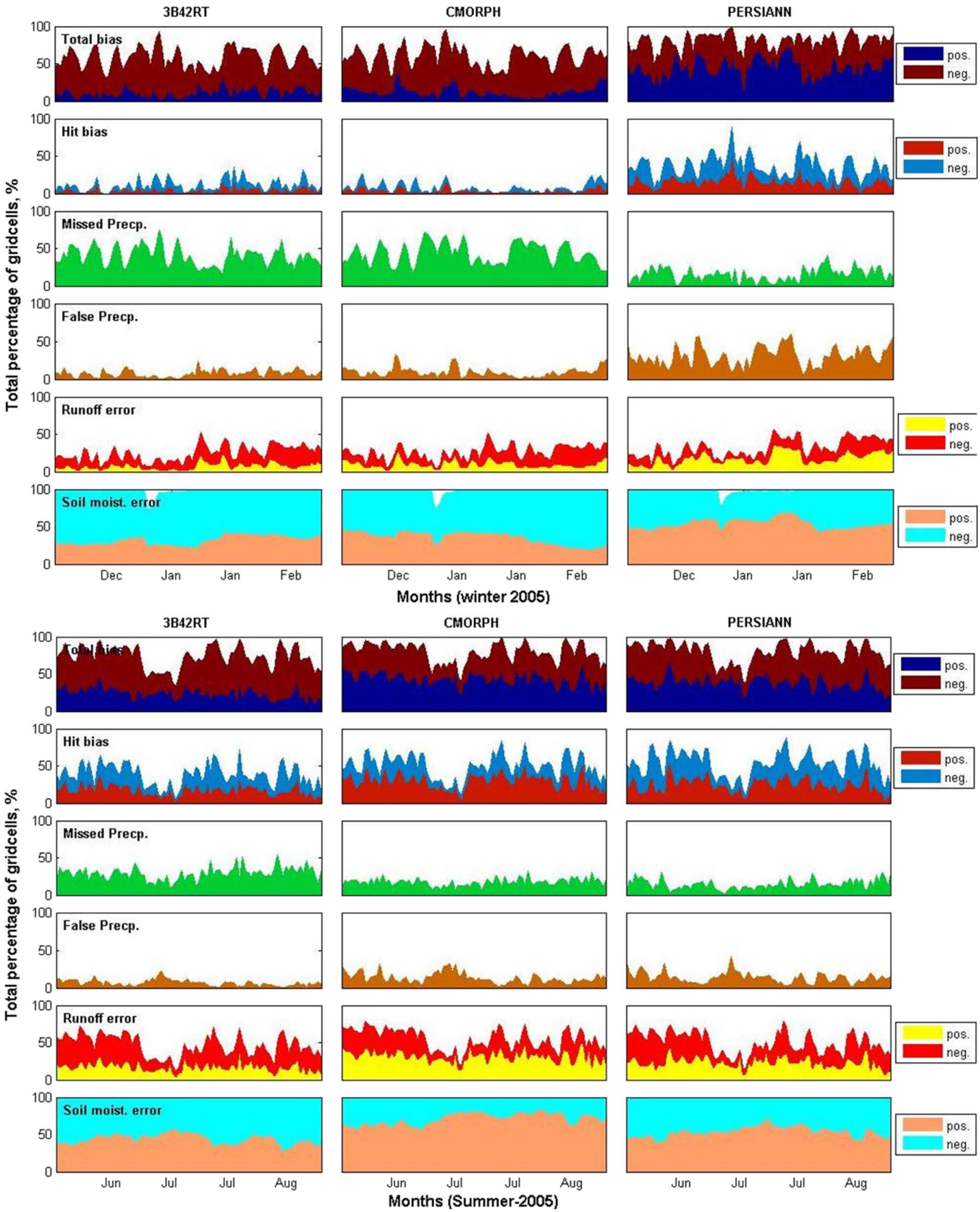

Fig. 8. Same as Fig. 7, except highland region (NOTE: pos.—postive; neg.—negative).

Fig. 9 demonstrates the fraction of magnitude of each rainfall error component as a ratio of total bias for lowland (upper panel) and highland (lower panel) regions during winter and summer seasons. For 3B42RT, the largest magnitude of the error is missed precipitation. For CMORPH, the proportion of hit bias is considerably high for the summer season (74% and

TABLE III
SUMMARY OF PERCENTAGE OF PIXELS AFFECTED BY DIFFERENT ERRORS

	Error type		Winter			Summer		
			3B42RT	CMORPH	PERSIANN	3B42RT	CMORPH	PERSIANN
Lowland region	Total bias	*	56.6	56.7	71.0	65.2	67.4	77.7
		**	43.4	43.3	29.0	34.8	32.6	22.3
	Hit bias	*	19.6	23.7	37.3	32.9	40.7	50.0
	Miss-rain bias	*	35.4	31.3	16.1	29.8	21.9	12.7
	False-rain bias	*	1.7	1.8	17.6	2.5	4.7	15.1
	Runoff	*	45.5	45.8	54.2	45.2	47.8	51.0
		**	54.5	54.2	45.8	54.8	52.2	49.0
	Soil moisture	*	99.0	99.0	99.6	99.7	99.8	99.8
		**	1.0	1.0	0.4	0.3	0.2	0.2
Highland region	Total bias	*	48.0	55.5	79.0	62.7	69.4	74.1
		**	52.0	44.5	21.0	37.3	30.6	25.9
	Hit bias	*	9.0	11.4	28.2	26.9	40.6	45.3
	Miss-rain bias	*	29.3	26.9	10.1	30.3	16.6	11.9
	False-rain bias	*	9.7	17.2	40.7	5.5	12.2	17.0
	Runoff	*	20.8	28.9	39.8	37.3	46.3	44.1
		**	79.2	71.1	60.2	62.7	53.7	55.9
	Soil moisture	*	98.0	99.0	99.4	99.8	99.9	99.9
		**	2.0	1.0	0.6	0.2	0.1	0.1

* Error influenced pixels ** non- influenced pixels (no error)

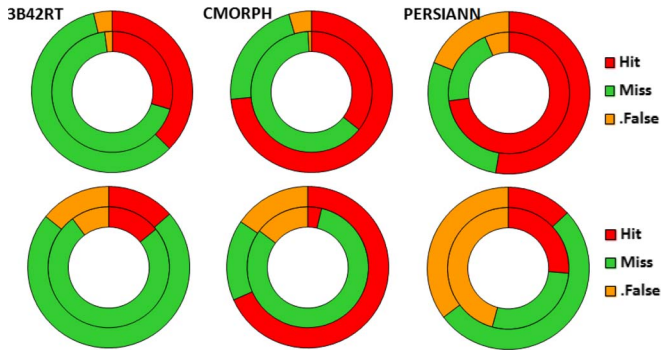

Fig. 9. Ratio of bias components to the total bias (HB/TB, MB/TB, and FB/TB, where HB is the hit bias, TB is the total bias, MB is the miss-rain bias, and FB is the false-rain bias), with the three ratios adding up to 1, for (upper panel) lowland and (lower panel) highland regions (NOTE: The inner circle is for winter, and the outer one is for summer season).

68% for lowland and highland, respectively). This shows that, during the rainy season, CMORPH overestimates the rainfall with noticeably high magnitude. In case of PERSIANN, the ratio of false precipitation is high during summer for lowland and high during winter for highland region (numerically, it is 20% and 69% for lowland and highland, respectively).

To demonstrate the relative contributions of terrain and climate feature, a more rigorous study is conducted by dividing pixels from the same elevation band among Koppen climate subclasses. Within a particular region, the dominant climate zones are only considered as shown in Figs. 1(d) and 10. Fig. 10 shows how much the terrain height and the climate are sensitive to the relationship between rainfall error components and hydrologic fluxes. First, except for region 5 (highland), the average percentage difference of correlation coefficients for climate subclasses is less than 15% for both runoff and soil moisture in all regions. This shows that, within the same topographic region, the climate type does not influence the correlation coefficients. The lengths of the bars in Fig. 10 illustrate little variation of coefficient of correlation for the leading error components (such as total bias, hit bias, and also missed-rain bias in the case of soil moisture). Second, the same climate classes that are found in different topographic regions do not have consistent correlation coefficients. This indicates that topography is a major controlling factor. On the other hand, climate type also plays a major role in highland region (region 5). The percentage difference of correlation coefficient in this region amounts to 70%. In highland regions, irrespective of the altitude, the rainfall variability is significant across windward and leeward sides of the mountain, resulting in uneven error characteristics.

IV. CONCLUSION AND RECOMMENDATION

In this paper, the total bias of satellite rainfall was decomposed into hit bias, miss-rain bias, and false-rain bias, and the nature of these error components, including runoff and soil moisture errors, was thoroughly investigated based on regions that were categorized by topography and Koppen climate classes. Based on topography, MRB was regionalized into five regions and, also based on Koppen climate type, into five dominant climate classes (see Fig. 1). Perhaps the most revealing finding of this study is the dominance of topography over climate features on satellite rainfall uncertainty. This is not surprising because topography is also a governing factor for Koppen climate classification, and thus, to some extent, the geographic location and the layout of regions are similar for both classification scenarios. It appears therefore that the study of topography, by default, makes the inclusion of climate information somewhat redundant as no additional underlying and physical insights are revealed.

It was found that the hit bias and missed precipitation are the two leading error sources for the total bias for both the 3B42RT and CMORPH products. The missed precipitation was pervasive during the winter time, and the hit bias prevailed during the summer. For the PERSIANN product, the two principal error sources were false-rain bias and hit bias (hit bias being a common prime error for all products) for winter and summer seasons, respectively.

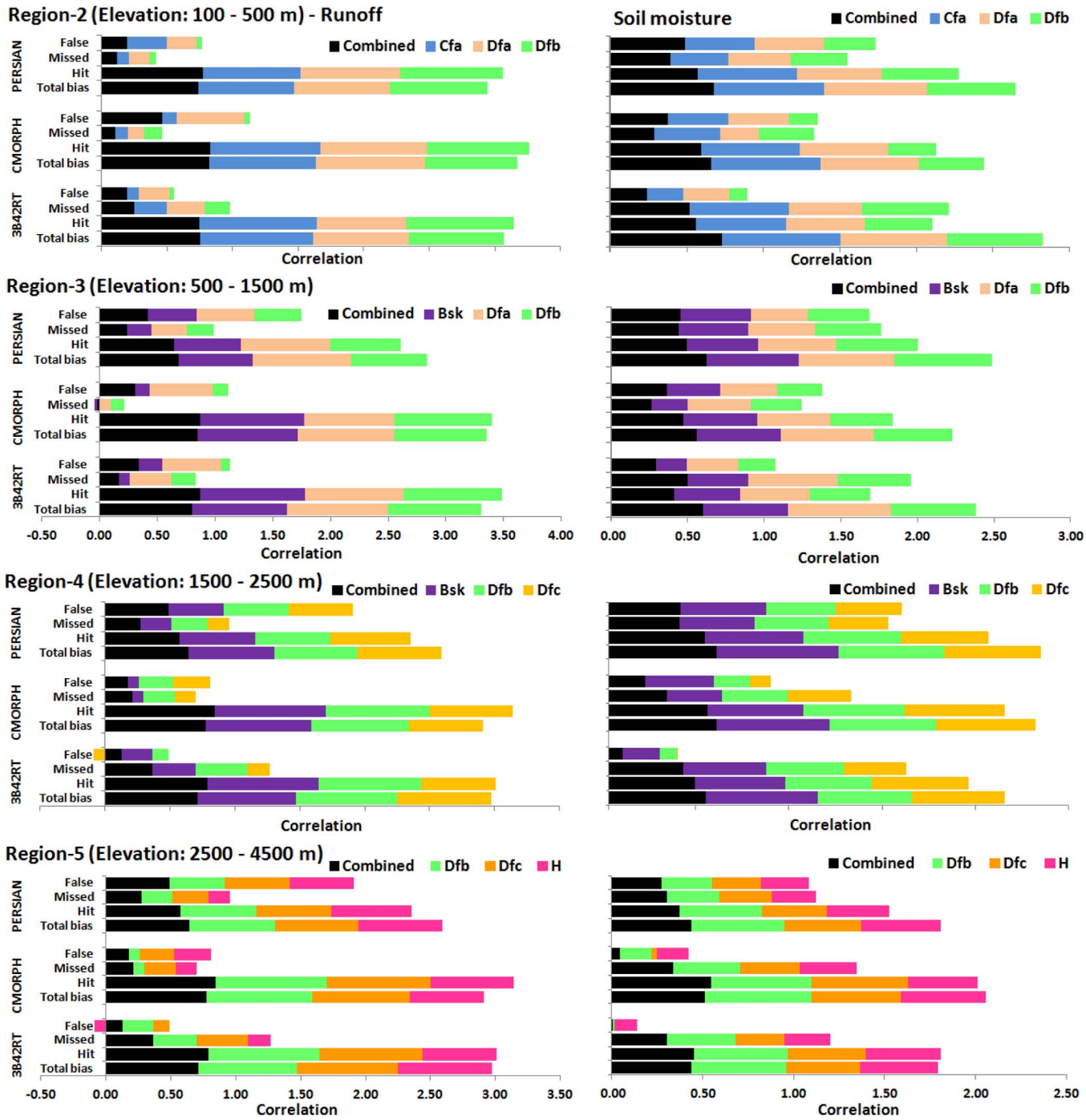

Fig. 10. Correlation coefficient of rainfall error components with (left panel) runoff and (right panel) soil moisture errors for different Koppen climate classes in regions 2, 3, 4, and 5. Region 1 is characterized only by a single climate type (Cfa). The black bar shows the correlation coefficient between errors for the entire region, whereas the other color bars show the correlation coefficient when the regions are subdivided into climate subclasses.

The temporal trend analysis proved that the simulated soil moisture and runoff errors were controlled by the total bias and hit bias, respectively. Runoff error did not depend on miss-rain bias because, usually, missed precipitation occurs due to relatively short-lived storms such as local convective type of rainfall (T-storms). Local thunderstorms actually generate significant runoff as the rain rates usually exceed infiltration capacity by a significant margin; however, the storms are so short lived and cover such a small geographic region that the overall impact is lost when looking at coarser scales in space and time. The results of this study can be summed up into the following key points.

1) Characterizing error information based on governing factors such as topography and climate types provides valuable information, similar to LULC [21], on satellite rainfall error characteristics and its reliability for hydrologic model simulation. By breaking down rainfall total bias into its distinct components, the source of errors propagated into hydrologic fluxes and states can be

traced. This information enables hydrologist to make correct prediction considering the product type, geographic location, and the season of the simulation.

2) The performance of the three satellite rainfall products varies based on the seasons and location. Each product exhibits distinct pros and cons that collectively justify the motivation for a further merged product (similar to [37]) based on *a priori* hydrologic model predictability. For example, 3B42RT has anomalously high missed precipitation and less hit bias and false-rain bias; CMORPH tends to have strong hit bias during summer, miss-rain bias during winter, and less false-rain bias; and PERSIANN has considerably strong false precipitation in highland regions, high hit bias, and small miss-rain bias. The problems of the missed and the false precipitation are linked with the lack of influential screening strategies, whereas hit bias and, in some cases, false-rain bias are related to weak physical correlation between signal and rain estimate.

One of the major limitations of this work is that the study period is not recent enough to reflect the present status of rainfall algorithms. The algorithms of 3B42RT and CMORPH used stable configuration of PMW sensors from 2003 to 2008 [15] with the exception of the Advanced Microwave Scanning Radiometer sensor that started operation in April 2004. On the other hand, according to the information obtained courtesy of 3B42RT algorithm developers, many of the sensors (such as NOAA15, NOAA16, and NOAA17) are currently phased out and replaced by other new satellite sensors such as NOAA18 and MetOp1. Likewise, several improvements have also been made on the CMORPH product, but the data have recently been reprocessed for the entire CMORPH history [49] after this manuscript was written. The reader should be aware, however, that the old version of the CMORPH data set has been used in this study. In general, the validity of the recommendations in the study depends on the extent of improvements that have been made on the rainfall algorithms. The other key limitation of our study is that a detailed physical (process-based) understanding of rainfall uncertainties is attainable only for regions that have ground-truth (gauged) data. However, satellite rainfall products are more valuable for data sparse or remote regions of the world. Therefore, a key concern is addressing the nature of errors in poorly instrumented regions. We hope to conduct a deeper rooted investigation of error to address this issue for the vast regions of the world lacking in ground validation rainfall data from *in situ* networks. The goal of this future study, which we hope to report soon, will be to convey the quality-controlled information from gauged basins to the ungauged basins located far apart in a logical and systematic way by leveraging *a priori* information on readily available geophysical features in anticipation of the Global Precipitation Measurement mission.

APPENDIX I

Let us assume that P_s is the precipitation estimate by the satellite, P_r is the reference (ground-truth) precipitation, TB is the total bias, HB is the hit bias, MB is the missed-rain bias, FB is the false-rain bias, and TH is the threshold value. For practical purpose, TH can be considered between 0 and 1 mm/day of rainfall [17]

$$\text{TB} = P_s - P_r$$

$$\text{If } P_s > \text{TH and } P_r > \text{TH, then HB} = P_s - P_r$$

$$\text{If } P_s \leq \text{TH and } P_r > \text{TH, then MB} = P_s - P_r = -P_r$$

$$\text{If } P_s > \text{TH and } P_r \leq \text{TH, then FB} = P_s - P_r = P_s$$

Therefore, to evaluate the error, it is important to develop the event mask for the respective error components as shown in the following:

Condition	Error component	Event mask H	M	F
$P_s > \text{TH}$ and $P_r > \text{TH}$	Hit	1	0	0
$P_s \leq \text{TH}$ and $P_r > \text{TH}$	Miss	0	1	0
$P_s > \text{TH}$ and $P_r \leq \text{TH}$	False	0	0	1
$P_s \leq \text{TH}$ and $P_r \leq \text{TH}$	No error	0	0	0

If the event masks are denoted as R_h, R_m, and R_f for hit, miss-rain, and false-rain components, respectively, then we can demonstrate that the sum of error components is equal to the total bias

$$\begin{aligned}\text{HB}+\text{MB}+\text{FB} &= (P_s - P_r)\times R_h + (-P_r)\times R_m + (P_s)\times R_f \\ &= P_s \times R_h - P_r \times R_h - P_r \times R_m + P_s \times R_f \\ &= P_s(R_h + R_f) - P_r(R_h + R_f)\end{aligned}$$

but from the event mask matrix above, one can understand that $R_h + R_f = R_h + R_f = 1$ for all conditions except $P_s \leq \text{TH}$ and $P_r \leq \text{TH}$ ("no error" condition).

Thus, $\text{HB}+\text{MB}+\text{FB} = P_s \times 1 - P_r \times 1 = P_s - P_r = \text{TB}$.

ACKNOWLEDGMENT

The authors graciously acknowledge the support and mentorship by Dr. C. Peters-Lidard and Dr. Y. Tian through NASA's 2011 Graduate Student Summer Program (GSSP) contributed to the design of the experiments conducted afterward at Tennessee Technological University. The authors are also thankful for the help received from the University of Washington Land Surface Hydrology group to handle the variable infiltration capacity hydrologic model and provide model input data sets. Passive microwave sensor information is provided courtesy of Dr. G. J. Huffman at the NASA Laboratory of Atmospheres/Science Systems and Applications, Inc.

REFERENCES

[1] B. Nijssen and D. P. Lettenmaier, "Effect of precipitation sampling error on simulated hydrological fluxes and states: Anticipating the global precipitation measurement satellites," *J. Geophys. Res.*, vol. 109, p. D02103, 2004. doi:10.1029/2003JD003497.

[2] Y. Hong, K.-L. Hsu, H. Moradkhani, and S. Sorooshian, "Uncertainty quantification of satellite precipitation estimation and Monte Carlo assessment of the error propagation into hydrologic response," *Water Resour. Res.*, vol. 42, p. W08421, 2006. doi:10.1029/2005WR004398.

[3] Y. Tian, C. D. Peters-Lidard, and J. B. Eylander, "Real-time bias reduction for satellite-based precipitation estimates," *J. Hydrometeorol.*, vol. 11, no. 6, pp. 1275–1285, Dec. 2010.

[4] C. Kummerow, W. S. Olson, and L. Giglio, "A simplified scheme for obtaining precipitation and vertical hydrometeor profiles from passive microwave sensors," *IEEE Trans. Geosci. Remote Sens.*, vol. 34, no. 5, pp. 1213–1232, Sep. 1996.

[5] R. J. Kuligowski, "A self-calibrating real-time GOES rainfall algorithm for short-term rainfall estimates," *J. Hydrometeorol.*, vol. 3, no. 2, pp. 112–130, Apr. 2002.

[6] T. Zhu and D. Zhang, "Impact of the advanced microwave sounding unit measurements on hurricane prediction," *Mon. Wea. Rev.*, vol. 130, no. 10, pp. 2416–2432, Oct. 2002.

[7] M. Demaria, M. Mainelli, L. K. Shay, J. A. Knaff, and J. Kaplan, "Further improvements to the Statistical Hurricane Intensity Prediction Scheme (SHIPS)," *Wea. Forecast.*, vol. 20, no. 4, pp. 531–543, Aug. 2005.

[8] E. I. Nikolopoulos, E. N. Anagnostou, F. Hossain, M. Borga, and M. Gebremichael, "Understanding the scale relationships of uncertainty propagation of satellite rainfall through a distributed hydrological model," *J. Hydrometeorol.*, vol. 11, no. 2, pp. 520–532, Apr. 2010.

[9] H. Taubenbock, M. Wurm, M. Netzband, H. Zwenzner, A. Roth, A. Rahman, and S. Dech, "Flood risks in urbanized areas—Multi-sensoral approaches using remotely sensed data for risk assessment," *Nat. Hazards Earth Syst. Sci.*, vol. 11, pp. 431–444, 2011.

[10] C. A. Reynolds, "Real-time hydrology operations at USDA for monitoring global soil moisture and auditing national crop yield estimates," in *Satellite Rainfall Applications for Surface Hydrology*, M. Gebremichael and F. Hossain, Eds. New York: Springer-Verlag, 2010, pp. 3–22.

[11] C. Funk and J. P. Verdin, "Real-time decision support systems: The famine early warning system network," in *Satellite Rainfall Applications for Surface Hydrology*, M. Gebremichael and F. Hossain, Eds. New York: Springer-Verlag, 2010, pp. 3–22.

[12] R. W. Reynolds, N. A. Rayner, T. M. Smith, D. C. Stokes, and W. Wang, "An improved in situ and satellite SST analysis for climate," *J. Clim.*, vol. 15, no. 3, pp. 1609–1625, Jul. 2002.

[13] Y. Fan and H. van den Dool, "Climate prediction center global monthly soil moisture data set at 0.5 ° resolution for 1948 to present," *J. Geophys. Res.*, vol. 109, p. D10102, 2004. doi:10.1029/2003JD004345.

[14] F. Su, Y. Hong, and D. P. Lettenmaier, "Evaluation of TRMM Multisatellite Precipitation Analysis (TMPA) and its utility in hydrologic prediction in the La Plata basin," *J. Hydrometeorol.*, vol. 9, pp. 622–640, 2008.

[15] Y. Hong, R. F. Adler, G. J. Huffman, and H. Pierce, "Applications of TRMM-based multi-satellite precipitation estimation for global runoff prediction: Prototyping a global flood modeling system," in *Satellite Rainfall Applications for Surface Hydrology*, M. Gebremichael and F. Hossain, Eds. New York: Springer-Verlag, 2010, pp. 3–22.

[16] M. Steiner, "Uncertainty of estimates of monthly areal rainfall for temporally sparse remote observations," *Water Resour. Res.*, vol. 32, no. 2, pp. 373–388, Feb. 1996.

[17] Y. Tian, C. D. Peters-Lidard, J. B. Eylander, R. J. Joyce, G. J. Huffman, R. F. Adler, K. Hsu, F. J. Turk, M. Garcia, and J. Zeng, "Component analysis of errors in satellite-based precipitation estimates," *J. Geophys. Res.*, vol. 114, p. D24101, 2009. doi:10.1029/2009JD011949.

[18] H. Moradkhani, K. L. Hsu, H. Gupta, and S. Sorooshian, "Uncertainty assessment of hydrologic model states and parameters: Sequential data assimilation using the particle filter," *Water Resour. Res.*, vol. 41, p. W05012, 2005. doi:10.1029/2004WR003604.

[19] E. I. Nikolopoulos, E. N. Anagnostou, and F. Hossain, "Error propagation of satellite-rainfall in flood prediction applications over complex terrain: A case study in Northeastern Italy," in *Satellite Rainfall Applications for Surface Hydrology*, M. Gebremichael and F. Hossain, Eds. New York: Springer-Verlag, 2010, pp. 3–22.

[20] E. Serpetzoglou, E. N. Anagnostou, A. Papadopoulos, E. I. Nikolopoulos, and V. Maggioni, "Error propagation of remote sensing rainfall estimates in soil moisture prediction from land surface model," *J. Hydrometeorol.*, vol. 11, no. 3, pp. 705–720, Jun. 2010.

[21] A. S. Gebregiorgis, C. D. Peters-Lidard, Y. Tian, and F. Hossain, "Tracing hydrologic model simulation error as a function of satellite rainfall estimation bias components and land use and land cover conditions," *Water Resour. Res.*, 2011, to be published.

[22] M. Steiner, T. L. Bell, Y. Zhang, and E. F. Wood, "Comparison of two methods for estimating the sampling-related uncertainty of satellite rainfall averages based on a large radar dataset," *J. Clim.*, vol. 15, pp. 3759–3778, 2003.

[23] G. J. Huffman, "Estimates of root-mean-square random error for finite samples of estimated precipitation," *J. Appl. Meteorol.*, vol. 36, no. 9, pp. 1191–2101, Sep. 1997.

[24] F. Hossain and E. N. Anagnostou, "A two-dimensional satellite rainfall error model," *IEEE Trans. Geosci. Remote Sens.*, vol. 44, no. 6, pp. 1511–1522, Jun. 2006.

[25] F. Hossain and G. J. Huffman, "Investigating uncertainty metrics for satellite rainfall at hydrologically relevant scales," *J. Hydrometeorol.*, vol. 9, pp. 563–575, 2008.

[26] Y. Tian and C. D. Peters-Lidard, "A global map of uncertainties in satellite-based precipitation measurements," *Geophys. Res. Lett.*, vol. 37, p. L24407, 2010. doi:10.1029/2010GL046008.

[27] L. Tang and F. Hossain, "Investigating the similarity of satellite rainfall error metrics as a function of Köppen climate classification," *Atmosp. Res.*, vol. 104/105, pp. 182–192, Feb. 2012.

[28] F. Hossain and E. N. Anagnostou, "Assessment of current passive-microwave- and infrared-based satellite rainfall remote sensing for flood prediction," *J. Geophys. Res.*, vol. 109, p. D07102, 2004. doi:10.1029/2003JD003986.

[29] T. J. Hewison, "Airborne measurements of forest and agricultural land surface emissivity at millimeter wavelengths," *IEEE Trans. Geosci. Remote Sens.*, vol. 39, no. 2, pp. 393–400, Feb. 2001.

[30] A. M. Anders, G. H. Roe, B. Hallet, D. R. Montgomery, N. J. Finnegan, and J. Putkonen, "Spatial patterns of precipitation and topography in the Himalaya," in *Tectonics, Climate, and Landscape Evolution: Geological Society of America Special Paper*, vol. 398, S. D. Willett, N. Hovius, M. T. Brandon, and D. Fisher, Eds. Boulder, CO: Geol. Soc. Amer., 2006, pp. 39–53.

[31] S. E. Nicholson, B. Some, J. Mccollum, E. Nelkin, D. Klotter, Y. Berte, B. M. Diallo, I. Gaye, G. Kpabeba, O. Ndiaye, J. N. Noukpozounkou, M. M. Tanu, A. Thiam, A. A. Toure, and A. K. Traore, "Validation of TRMM and other rainfall estimates with a high-density gauge dataset for West Africa. Part II: Validation of TRMM rainfall products," *J. Appl. Meteorol.*, vol. 42, no. 10, pp. 1355–1367, Oct. 2003.

[32] T. Dinku, P. Ceccato, E. Grover-Kopec, M. Lemma, S. J. Connor, and C. F. Ropelewski, "Validation of satellite rainfall products over East Africa's complex topography," *Int. J. Remote Sens.*, vol. 28, no. 7, pp. 1503–1526, Mar. 2007.

[33] T. Dinku, S. J. Connor, and P. Ceccato, "Comparison of CMORPH and TRMM-3B42 over mountainous regions of Africa and South America," in *Satellite Rainfall Applications for Surface Hydrology*, M. Gebremichael and F. Hossain, Eds. New York: Springer-Verlag, 2010, pp. 193–204.

[34] A. Gruber and V. Levizzani, Assessment of Global Precipitation Products, WMO/TD-NO. 1430, 2008. [Online]. Available: http://wcrp.wmo.int/documents/AssessmentGlobalPrecipitationReport.pdf

[35] F. A. Hirpa, M. Gebremichael, and T. Hopson, "Evaluation of high resolution satellite precipitation products over very complex terrain in Ethiopia," *J. Appl. Meteorol. Clim.*, vol. 49, no. 5, pp. 1044–1051, May 2010. doi:10.1175/2009JAMC2298.1.

[36] J. P. Giovannettone and A. P. Barros, "Probing regional orographic controls of precipitation and cloudiness in the Central Andes using satellite data," *J. Hydrometeorol.*, vol. 10, no. 1, pp. 167–182, Feb. 2009.

[37] A. S. Gebregiorgis and F. Hossain, "How much can *a priori* hydrologic model predictability help in optimal merging of satellite precipitation products?" *J. Hydrometeorol.*, vol. 12, no. 6, pp. 1287–1298, Dec. 2011. doi: 10.1175/JHM-D-10-05023.1.

[38] M. C. Peel, B. L. Finlayson, and T. A. McMahon, "Updated world map of the Köppen–Geiger climate classification," *Hydrol. Earth Syst. Sci.*, vol. 11, pp. 1633–1644, 2007.

[39] X. Liang, D. P. Lettenmaier, E. F. Wood, and S. J. Burges, "A simple hydrologically based model of land surface water and energy fluxes for GSMs," *J. Geophys. Res.*, vol. 99, no. D7, pp. 14 415–14 428, 1994.

[40] E. P. Maurer, A. W. Wood, J. C. Adam, D. P. Lettenmaier, and B. Nijssen, "A long-term hydrologically based dataset of land surface fluxes and states for the conterminous United States," *J. Clim.*, vol. 15, no. 22, pp. 3237–3251, Nov. 2002.

[41] E. Habib, B. F. Larson, and J. Graschel, "Validation of NEXRAD multisensor precipitation estimates using an experimental dense rain gauge network in South Louisiana," *J. Hydrol.*, vol. 373, no. 3/4, pp. 463–478, Jul. 2009.

[42] G. J. Huffman, R. F. Adler, D. T. Bolvin, and E. J. Nelkin, "The TRMM Multisatellite Precipitation Analysis (TMPA)," in *Satellite Rainfall Applications for Surface Hydrology*, M. Gebremichael and F. Hossain, Eds. New York: Springer-Verlag, 2010, pp. 3–22.

[43] G. J. Huffman, R. F. Adler, D. T. Bolvin, G. Gu, E. J. Nelkin, K. P. Bowman, Y. Hong, E. F. Stocker, and D. B. Wolff, "The TRMM multisatellite precipitation analysis: Quasi-global, multi-year, combined sensor precipitation estimates at fine scale," *J. Hydrometeorol.*, vol. 8, pp. 38–55, 2007.

[44] R. Joyce, J. E. Janowiak, P. A. Arkin, and P. Xie, "CMORPH: A method that produces global precipitation estimates from passive microwave and infrared data at high spatial and temporal resolution," *J. Hydrometeorol.*, vol. 5, no. 3, pp. 487–503, Jun. 2004.

[45] S. Sorooshian, K. L. Hsu, X. Gao, H. V. Gupta, B. Imam, and D. Braithwaite, "Evaluation of PERSIANN system satellite based estimates of tropical rainfall," *Bull. Amer. Meteorol. Soc.*, vol. 81, no. 9, pp. 2035–2046, 2000.

[46] Y. Hong, K. L. Hsu, S. Sorooshian, and X. Gao, "Precipitation estimation from remotely sensed information using artificial neural network cloud classification system," *J. Appl. Meteorol.*, vol. 43, no. 12, pp. 1834–1853, Dec. 2004.

[47] Y. Hong, K. Hsu, S. Sorooshian, and X. Gao, "Self-organizing nonlinear output (SONO): A neural network suitable for cloud patch-based rainfall estimation at small scales," *Water Resour. Res.*, vol. 41, p. W03008, 2005. doi:10.1029/2004WR003142.

[48] K. Hsu, A. Behrangi, B. Imam, and S. Sorooshian, "Extreme precipitation estimation using satellite-based PERSIANN-CCS algorithm," in *Satellite Rainfall Applications for Surface Hydrology*, M. Gebremichael and F. Hossain, Eds. New York: Springer-Verlag, 2010, pp. 49–67.

[49] R. J. Joyce, P. Xie, Y. Yarosh, J. E. Janowiak, and P. A. Arkin, "CMORPH: A 'morphing' approach for high resolution precipiation product generation," in *Satellite Rainfall Applications for Surface Hydrology*, M. Gebremichael and F. Hossain, Eds. New York: Springer-Verlag, 2010, pp. 23–37.

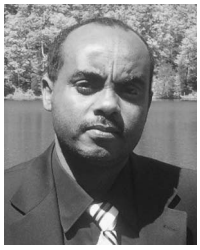

Abebe S. Gebregiorgis received the B.Sc. degree in hydraulic engineering from the Arba Minch Water Technology Institute, Arba minch, Ethiopia, in 2002 and the M.Sc. degree in hydraulic and hydropower engineering from Arba Minch University, Arba minch, in 2004. He is currently working toward the Ph.D. degree in civil and environmental engineering at Tennessee Technological University, Cookeville.

His field of research is on hydrologically relevant and optimal merging of high-resolution satellite precipitation products to enhance macroscale hydrologic modeling application.

Faisal Hossain received the Ph.D. degree from the University of Connecticut, Storrs, in 2004. Prior to that, he had received the M.S. degree from the National University of Singapore, Singapore and the B.S. degree from the Indian Institute of Technology, Varanasi (IT-BHU), India.

He is currently an Associate Professor with the Department of Civil and Environmental Engineering, Tennessee Technological University, Cookeville, where he received one of highest awards of the university—the Caplenor Research Award in 2012. His research interests comprise hydrologic remote sensing, uncertainty modeling of water cycle variables, human modification of extreme hydroclimatology, sustainable water resource engineering, spaceborne transboundary water resource management, engineering education, and public outreach. He has published over 85 peer-reviewed journal articles, authored an undergraduate-level textbook, edited two book volumes, and contributed eight book chapters. His recent research on human modification of extreme events by artificial reservoirs has been featured by public media such as the BBC, National Geographic, New Scientist, Newsweek, Fox News, MSNBC, Wired.com, and German Public Radio. He served as an Associate Editor of the *Journal of American Water Resources Association* from 2006 to 2010. Currently, he serves as an Associate Editor for the *Journal of Hydrometeorology* and Lead Editor for the water volume of the Elsevier Sciences 5 volume reference series on "Climate Vulnerability: Understanding and Addressing Threats to Essential Resources."

Dr. Hossain was the recipient of awards such as the NASA Earth System Science Fellowship (2002), the Outstanding Ph.D. Thesis Award (2005), the NASA New Investigator Award (2008), the American Society of Engineering Education Outstanding Research Award (2009), the National Association of Environmental Professionals Education Excellence Award (2010), the U.S. Fulbright Faculty Award (2012), and the Graduate of the Last Decade Award from the University of Connecticut (2012).